
SkyDiffusion: Street-to-Satellite Image Synthesis with Diffusion Models and BEV Paradigm

Junyan Ye^{1,2}, Jun He¹, Weijia Li^{1*}, Zhutao Lv¹, Jinhua Yu¹,
Haote Yang², Conghui He^{2,3*}

¹Sun Yat-Sen University, ²Shanghai AI Laboratory, ³Sensetime Research
{yejy53, hejun36, lvzht5, yujh56}@mail2.sysu.edu.cn,
liweij29@mail.sysu.edu.cn, {yanghaote, heconghui}@pjlab.org.cn

Abstract

Street-to-satellite image synthesis focuses on generating realistic satellite images from corresponding ground street-view images while maintaining a consistent content layout, similar to looking down from the sky. The significant differences in perspectives create a substantial domain gap between the views, making this cross-view generation task particularly challenging. In this paper, we introduce SkyDiffusion, a novel cross-view generation method for synthesizing satellite images from street-view images, leveraging diffusion models and Bird's Eye View (BEV) paradigm. First, we design a Curved-BEV method to transform street-view images to the satellite view, reformulating the challenging cross-domain image synthesis task into a conditional generation problem. Curved-BEV also includes a "Multi-to-One" mapping strategy for combining multiple street-view images within the same satellite coverage area, effectively solving the occlusion issues in dense urban scenes. Next, we design a BEV-controlled diffusion model to generate satellite images consistent with the street-view content, which also incorporates a light manipulation module to optimize the lighting condition of the synthesized image using a reference satellite. Experimental results demonstrate that SkyDiffusion outperforms state-of-the-art methods on both suburban (CVUSA & CVACT) and urban (VIGOR-Chicago) cross-view datasets, with an average SSIM increase of 14.5% and a FID reduction of 29.6%, achieving realistic and content-consistent satellite image generation. The code and models of this work will be released at <https://opendatalab.github.io/skydiffusion/>.

1 Introduction

Cross-view synthesis involves transformations between disparate viewpoints, such as from street-view images to satellite images and vice versa. This process is crucial for applications in autonomous driving [2], 3D reconstruction [40, 7], virtual reality [3, 6], etc. The significant changes in street view and satellite perspectives result in drastically different appearances of objects, leading to a substantial disparity between different image domains. As shown in Fig 1 (a), in cross-view scenarios, building facades observed only in street view and rooftops observed only from satellite view are considered uncorrelated and drastically different features [24, 35, 47]. However, objects such as roads and lawns, which are below the viewpoint, can be observed in different views even if they undergo some deformation, making them cross-view shared correlated information. The key to the challenging task of cross-view generation lies in capturing cross-view relevant information and generating realistic views with consistent content layout.

*W. Li and C. He are the corresponding authors.

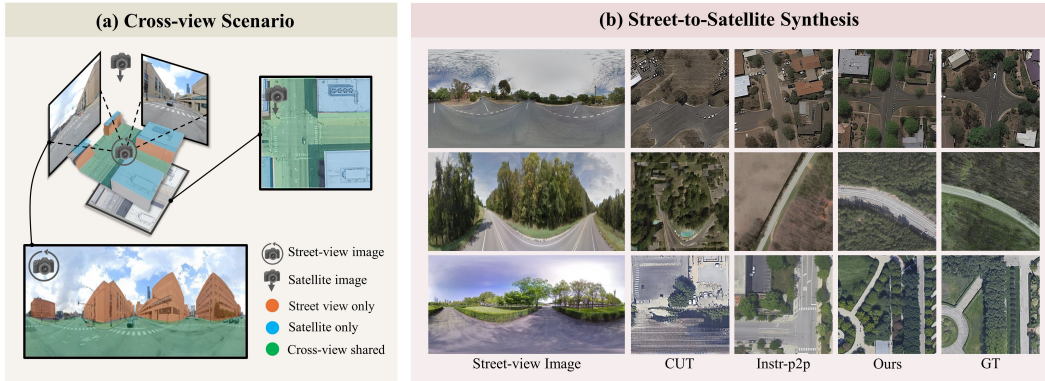


Figure 1: Illustration of the cross-view image synthesis task. (a) In the cross-view scenario, there are features unique to the street-view image, features exclusive to the satellite image, and shared correlated information observable from both views. (b) Comparison with existing methods using GANs (e.g., CUT [21]) or diffusion models (e.g., Instr-p2p [1]) for street-to-satellite image synthesis.

In the field of cross-view synthesis, converting satellite images to street-view images has received extensive attention [30, 20, 43, 23]. Researchers have leveraged polar transformations [38, 31] or geo-transformation [20] to bridge the gap from the satellite to the street view domain, and then employ Generative Adversarial Networks (GANs) to generate realistic street views. This paper focuses on the less explored yet equally challenging task of synthesizing satellite images from street-view images. Some researchers have used semantic segmentation priors to aid in synthesizing satellite images, achieving notable results [24, 35]. However, the semantic maps are often unavailable in real scenarios. Existing street-to-satellite image generation also lacks transformations such as polar or geo-transformation to fit the gap from the street view to the satellite domain. Moreover, as shown in Fig 1(b), existing methods on street-to-satellite image synthesis, which mostly rely on GANs, often result in lower-quality satellite images with unrealistic textures compared to the ground truth (GT).

Recently, diffusion models have gained attention for their exceptional image synthesis and rich 3D world knowledge derived from large-scale text and 2D image data [9, 45]. Many studies have explored text-guided fine-tuning of diffusion models to top-down perspective from other views [15, 14, 11, 27]. Additionally, novel view synthesis methods have been developed by training with multi-view images and camera poses [19, 29]. Although current novel view synthesis techniques demonstrate satisfactory performance at the object level, their performance in cross-view generation for complex scenes with significant viewpoint differences remains suboptimal. A possible solution is to treat this task as an image translation task [16, 22, 1]. However, as shown in Fig 1(b), due to the domain gap of different views, the resulting images are often realistic but not actual, with significant discrepancies between the synthesized satellite images and the actual corresponding street view content.

In response to these challenges, this paper introduces SkyDiffusion, the first diffusion-model-based method for synthesizing satellite images from street-view images, similar to looking down from the sky. In SkyDiffusion, we design a curved-BEV method that transforms street-view images into the satellite view to achieve domain alignment between different views. Curved-BEV also includes a "Multi-to-One" BEV mapping method that can optimize BEV perception in densely occluded urban scenarios. Subsequently, we design a BEV-controlled diffusion model to generate satellite images consistent with the street-view content, incorporated with a light manipulation module to address the lack of inherent correlation in lighting conditions between the two views. SkyDiffusion outperforms existing state-of-the-art methods on both suburban (CVUSA and CVACT) and urban (VIGOR-Chicago) cross-view datasets, with an average SSIM increase of 14.5% and a FID reduction of 29.6%, successfully generating realistic and content-consistent satellite images.

2 Related Work

Cross-view image synthesis. Cross-view image synthesis involves generating realistic scene images with significant viewpoint changes, primarily divided into satellite-to-street [30, 20, 43, 23, 38] and street-to-satellite generation [35, 24, 25]. In this field, synthesizing satellite images from street views

is a challenging yet important task. Tang [35] used street-view images and aerial semantic maps for image-to-image translation to synthesize target satellite images, but semantic maps are often unavailable in real scenarios. Regmi [24] attempted to synthesize aerial views from a single street image, but the significant domain differences led to inconsistencies. Additionally, the performance of GANs has also limited the quality of street-to-satellite image synthesis in previous studies.

BEV transformation. BEV transformation is a perspective domain conversion technique similar to polar transformation [31, 38] and geo-transformation [20], widely used in retrieval [4], navigation [17] and localization tasks [34, 41, 32]. Traditional BEV transformation techniques, which rely on camera parameters [28] or depth estimation methods [37, 44], face challenges such as the difficulty in obtaining camera parameters and the high computational cost of depth estimation. Recently, some methods have been proposed to map street-view images to the BEV perspective using geometric relations at the image [41] or feature level [32]. However, such methods are based on the ground plane assumption, where all mapped points are located below the camera, limiting the mapping of upper street scene features and causing information loss. Furthermore, to our knowledge, no studies have yet explored the use of BEV methods for the task of street-to-satellite image generation.

Novel view synthesis based on diffusion models. Diffusion models have shown significant potential in recent studies on novel view synthesis [11, 15, 36, 5, 39]. DreamBooth [27] and AerialDiffusion [14] utilize text guidance to achieve top-down image generation by fine-tuning diffusion models. However, it is challenging to fully encapsulate the complexity of real-world scenes using textual information alone. Zero-1-to-3 [19] and Zero 123++ [29] use multi-view images and camera poses to guide diffusion models in learning object structures and textures, enabling new viewpoint synthesis. However, these methods are limited to object-level tasks with strong viewpoint correlations and struggle to handle the significant viewpoint changes in cross-view generation. Besides, diffusion-based image-to-image translation methods can also generate realistic satellite images [16, 1, 22, 45]. However, the substantial domain gap between street-view images and satellite images presents a significant challenge in generating content-consistent satellite images.

3 Method

As illustrated in Fig. 2, this paper introduces a novel method for synthesizing satellite images from corresponding street-view images. Our cross-view synthesis network, SkyDiffusion, initially applies a curved BEV transformation to the input street-view images, converting the perspective to a top-down view using either one-to-one or multi-to-one mappings (Section 3.1). Subsequently, the BEV-Controlled diffusion model with light manipulation is employed for the controlled synthesis of satellite images (Section 3.2). Following this, we detail our network training process (Section 3.3).

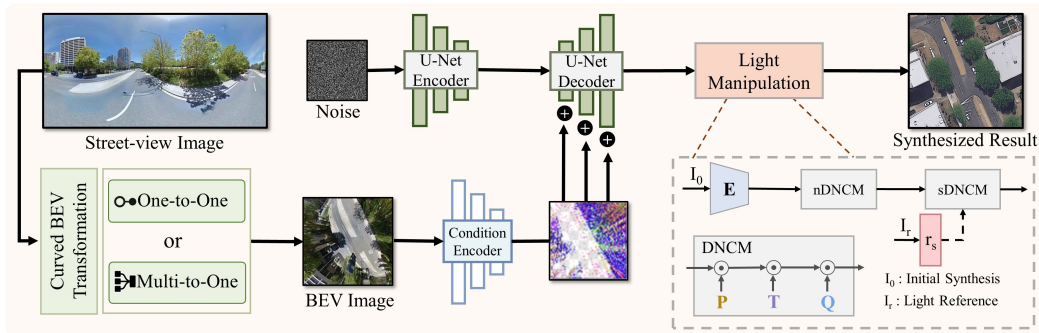


Figure 2: Overview of the proposed SkyDiffusion framework, including the curved BEV transformation and BEV-controlled diffusion model with light manipulation.

3.1 Curved BEV Transformation

One-to-One BEV. Existing BEV methods based on ground plane assumptions ($P(x, y, z = 0)$) and geometric relationships achieve the mapping from street view to the BEV plane[32, 41]. However, this assumption fails to map the content above the street-view image and results in noticeable distortion as

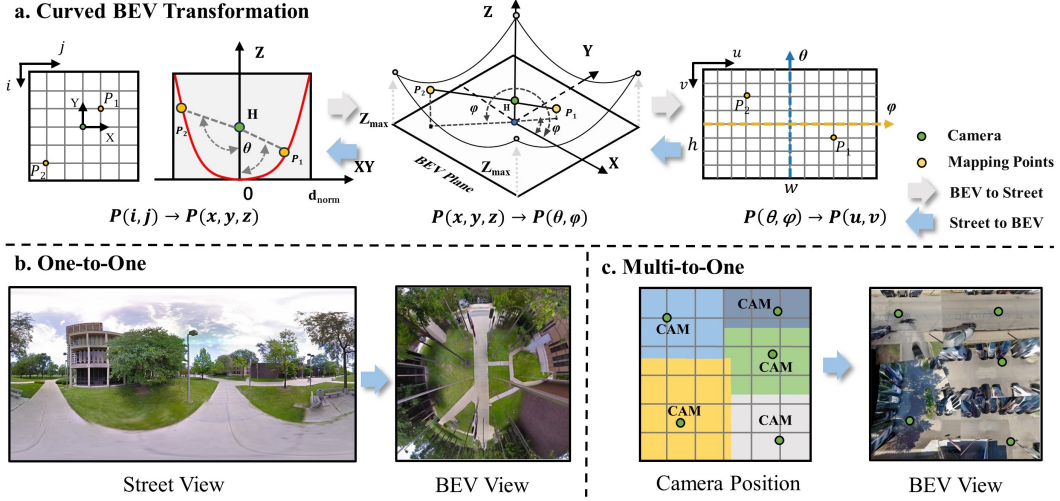


Figure 3: Schematic of the curved BEV transformation. The upper part (a) details the transformation process, highlighting the two mapping points at the top and bottom of the street view. The lower parts (b) and (c) present the results of One-to-One and Multi-to-One BEV transformations, respectively.

points move away from the center area. Thus, we propose an improved curved BEV transformation to alleviate this problem and better capture cross-view relevant information.

As shown in Fig. 3 (a), we use $P(i, j)$ to denote an index on the BEV space, and $P(x, y, z)$ to illustrate a point in a three-dimensional coordinate system with the camera on the z -axis. We assume that the BEV plane is an upward curved surface, with the height (z -axis) increasing rapidly as the 3D points move away from the center (the central part of Fig 3(a)). The following equation formulates the relationship between $P(x, y, z)$ and $P(i, j)$, where d_{norm} represents the normalized distance from the center, d_{max} is the maximum distance from the center, and λ is a scaling factor.

$$\begin{cases} x = j - \frac{l}{2}, & y = \frac{l}{2} - i \\ z = d_{norm}^4 \times \lambda = \left(\frac{\sqrt{x^2 + y^2}}{d_{max}} \right)^4 \times \lambda \end{cases} \quad (1)$$

Furthermore, we can convert $P(x, y, z)$ to spherical coordinates $P(\theta, \varphi)$. Based on the equirectangular projection properties of street view images, $P(\theta, \varphi)$ corresponds to the panorama image index $P(u, v)$. This allows us to establish the mapping relationship between $P(x, y, z)$ and $P(u, v)$ from the following equation, where H represents the camera height, and w, h represent the width and height of the street image. More details can be found in the supplementary material.

$$\begin{cases} u = [\arctan2(y, x) + \pi] \frac{w}{2\pi} \\ v = \left[\frac{\pi}{2} + \arctan2(z - H, \sqrt{x^2 + y^2}) \right] \frac{h}{\pi} \end{cases} \quad (2)$$

Following Eq. 1 and Eq. 2, we achieve the projection from the street-view image to the bird's eye view without requiring camera calibration parameters or depth estimation methods [28, 37, 44] (Fig. 3 (b)). This allows effective mapping of upper street view features, such as distant roads and buildings. Since the mapping relationship for each transformation is fixed, the computational overhead is minimal.

Multi-to-One BEV. Due to the limitations imposed by dense buildings on street view observations, the BEV sensing range is very limited in urban datasets like VIGOR [46]. To address this, we propose a "Multi-to-one" BEV mapping method that unifies multiple street view BEV mappings results BEV_{cam_k} into a single satellite coordinate system based on the relationships of camera position (Fig. 3 (c)). Additionally, we use a simple semantic segmentation network to identify and discard the regions with severe BEV distortion, typically those obstructed by buildings. We select the street view

mapping result closest to the capture point for overlapping areas following Eq. 3, where $BEV(x, y)$ represents the unified BEV space corresponding to the satellite image, x, y corresponds to the index position of the BEV plane, Δx_k and Δy_k represent the offset of the street-view image from the satellite center, and x_{cam_i} and y_{cam_i} represent the coordinates of camera position in the satellite coordinate system.

$$BEV(x, y) = BEV_{cam_k}(x - \Delta x_k, y - \Delta y_k), k = \arg \min_i \sqrt{(x - x_{cam_i})^2 + (y - y_{cam_i})^2} \quad (3)$$

This allows us to synthesize large-scale scenes using street-view images that typically contain only limited local information.

3.2 BEV-Controlled Diffusion Model with Light Manipulation

Curved BEV controlled synthesis. Image diffusion models learn to progressively denoise images and generate samples from the training domain. The denoising process can occur in pixel space or in a latent space encoded from training data. Inspired by ControlNet [45], we enhance the control over the generated aerial views by replicating the SD module, enabling the transformed BEV images to effectively guide the synthesis process. Specifically, we first use a small encoder to capture the cross-view associative information of the input BEV image I_{bev} such as road directions and building positions, to achieve BEV image feature embedding c_{bev} . Notably, considering the potential feature distortions in BEV images, we employ a spatial attention mechanism to enhance feature capture while suppressing distorted features.

$$c_{bev} = \mathcal{E}(I_{bev}). \quad (4)$$

Subsequently, by employing zero convolution layers and replicating the structures and weights of the encoder and middle block from the SD module, the extracted BEV features are injected into another SD module. Guided by the BEV image, the diffusion model considers cross-view associative information, synthesizing aerial views with consistent content.

Light Manipulation. Given the differences in perspectives and timing between satellite and street images, there is no direct correlation in lighting conditions. We employ the DNCM for modeling deterministic color mapping [12]. Initially, we use nDNCM to obtain the "image content information" I_c from the preliminary synthesis results I_0 of the satellite images. Then, we input the lighting and color style r_s obtained from the reference aerial view into sDNCM for lighting transfer.

$$I_s = sDNCM(nDNCM(I_0, I_c), r_s), \text{ where } DNCM(I, T) = (I_{h \times w, 3} \cdot P_{3,k}) \cdot T_{k,k} \cdot Q_{k,3} \quad (5)$$

I_c and r_s are the content information and color reference information extracted by the encoder E , as shown in Fig. 2. The DNCM module internally includes $P_{3,k}$ and $Q_{k,3}$, which represent the color embedding and recovery matrices, respectively. Here, k represents the embedding dimension. The adaptive color mapping matrix $T_{k,k}$ is also obtained through the encoder.

3.3 Network Training

Loss Function. We train the BEV-controlled synthesis of satellite images and the light manipulation module in two separate stages. Given a set of cross-view image data, the image diffusion algorithm gradually adds noise to the satellite image, generating a noisy satellite image Z_t . It then learns a network ϵ_θ to predict the noise added to the noisy satellite image Z_t based on the given BEV image as the conditional input. Since text cannot fully describe the street view scene, our cross-view image synthesis is essentially an image-conditioned synthesis task, with text not being our optimization target. This helps the model focus on generating satellite images based on the BEV conditions.

$$\mathcal{L} = \mathbb{E}_{sat_0, t, c_{bev}, \epsilon \sim \mathcal{N}(0,1)} \left[\|\epsilon - \epsilon_\theta(sat_t, t, c_{bev})\|_2^2 \right] \quad (6)$$

The loss \mathcal{L} is the learning objective of the diffusion model, where t represents the time step.

Following previous image migration work [13, 12], we apply different LUT filters to the satellite images to simulate the results under various lighting conditions for training the light manipulation module. During training, we use L2 consistency loss \mathcal{L}_{con} to maintain image content consistency and L1 reconstruction loss \mathcal{L}_{rec} to learn color style transfer.

Implementation Details. We implement SkyDiffusion using the pre-trained Stable Diffusion v1.5 model [26], with an unlocked diffusion decoder and a classifier-free guidance scale of 9.0 [10]. Final inference sampling uses 50 steps with the DDIM strategy[33]. Training is on eight NVIDIA A100 GPUs with a batch size of 128 for 100 epochs. In the curved BEV transformation, the parameter λ is set to 15 and H is set to 1.5. For light manipulation, the reference satellite image is randomly selected from normally toned images in the training set, as shown in Figure 8, and the DNCM mapping matrix parameter k is set to 32 (details in Supplementary Material).

4 Experiments

In this section, we introduce the three datasets utilized and the experimental setup. We then conduct both qualitative and quantitative comparisons of SkyDiffusion with state-of-the-art cross-view synthesis methods. Finally, we perform ablation studies to evaluate the effectiveness of each module.

4.1 Datasets

Suburban dataset (CVUSA & CVACT) are two commonly used cross-view datasets, containing centrally aligned aerial and street-view images from regions in the United States and Canberra, Australia, respectively, in a one-to-one mapping relationship. The data primarily consists of suburban scenes with relatively low-rise buildings and open views. The CVUSA dataset’s training and testing sets are randomly split, while the CVACT dataset is split by region.

Urban dataset (VIGOR-Chicago) is a subset of the VIGOR dataset, containing cross-view image pairs collected from Chicago. In this dataset, the street panorama and satellite images are not centrally aligned, and multiple street-view images cover the same satellite image area, with overlapping regions between different satellite images, forming a many-to-one mapping relationship.

In CVUSA [42], the street-view image is 256×1024 pixels, while in CVACT [18] and VIGOR [46], it is 512×1024 , all with north in the central column. Unlike previous methods that synthesize low-resolution satellite images (64×64 or 256×256 pixels), this experiment aims to meet practical needs by generating higher-resolution satellite images (512×512 pixels). The images obtained from street images after the Curved-BEV transformation are the same size as the satellite images.

4.2 Experimental Setup

We compare our approach on three datasets with several state-of-the-art cross-view synthesis methods, including GAN-based methods like X-Seq [24], CUT [21], and CDTE [38], and diffusion models for image translation like img2img-turbo [22] and Instruct pix2pix (Instr-p2p) [1]. We also compare with fine-tuned diffusion models for novel view generation, including DreamBooth [27], Aerial Diff [14], and HawkI [15]. Except for the fine-tuned diffusion models, which use a brief textual description, all other models use the same street-view input for a fair comparison. Following previous work [20, 38, 24], we employ commonly used metrics such as SSIM, PSNR and LPIPS to evaluate the content consistency of the synthesized images, and use FID [8] to assess the realism of images.

4.3 Comparison with State-of-the-Art Methods

On the suburban CVUSA and CVACT datasets, our SkyDiffusion method achieves the best results, with a 28.4% reduction in FID and a 17.4% improvement in SSIM compared to the state-of-the-art, demonstrating its superiority in synthesizing realistic and consistent and satellite images. The visual results in Fig. 4 show that GAN-based cross-view methods generate excessive artifacts and blurriness. While diffusion-based methods such as Aerial Diff [14] and Instr-p2p [1] produce highly realistic aerial views, they lack content correlation with the street-view images. In contrast, our method benefits from BEV perspective transformation, enabling effective capture of associative information. SkyDiffusion generates realistic images with consistent content layout, including road direction, tree placement, and building distribution.

Table 1: Quantitative comparison of different methods on CVUSA [42] and CVACT [18].

Method	CVUSA				CVACT			
	FID (↓)	SSIM (↑)	PSNR (↑)	LPIPS (↓)	FID (↓)	SSIM (↑)	PSNR (↑)	LPIPS (↓)
X-Seq [24]	161.16	0.084	11.97	0.706	190.12	0.042	12.41	0.661
CDTE [38]	122.84	0.143	10.01	0.694	160.81	0.091	12.59	0.663
CUT [21]	72.52	0.122	12.12	0.695	62.34	0.101	13.02	0.662
Aerial Diff [14]	136.18	0.103	10.06	0.855	127.29	0.108	10.24	0.878
DreamBooth [27]	102.99	0.103	11.31	0.812	88.12	0.107	12.81	0.791
Hawkl [15]	90.98	0.114	11.09	0.783	135.75	0.112	10.97	0.764
img2img-turbo [22]	77.95	0.103	12.64	0.685	73.24	0.103	12.19	0.679
Instr-p2p [1]	38.01	0.138	12.29	0.697	49.62	0.116	12.51	0.682
Ours	29.01	0.167	13.07	0.653	35.51	0.123	13.58	0.657

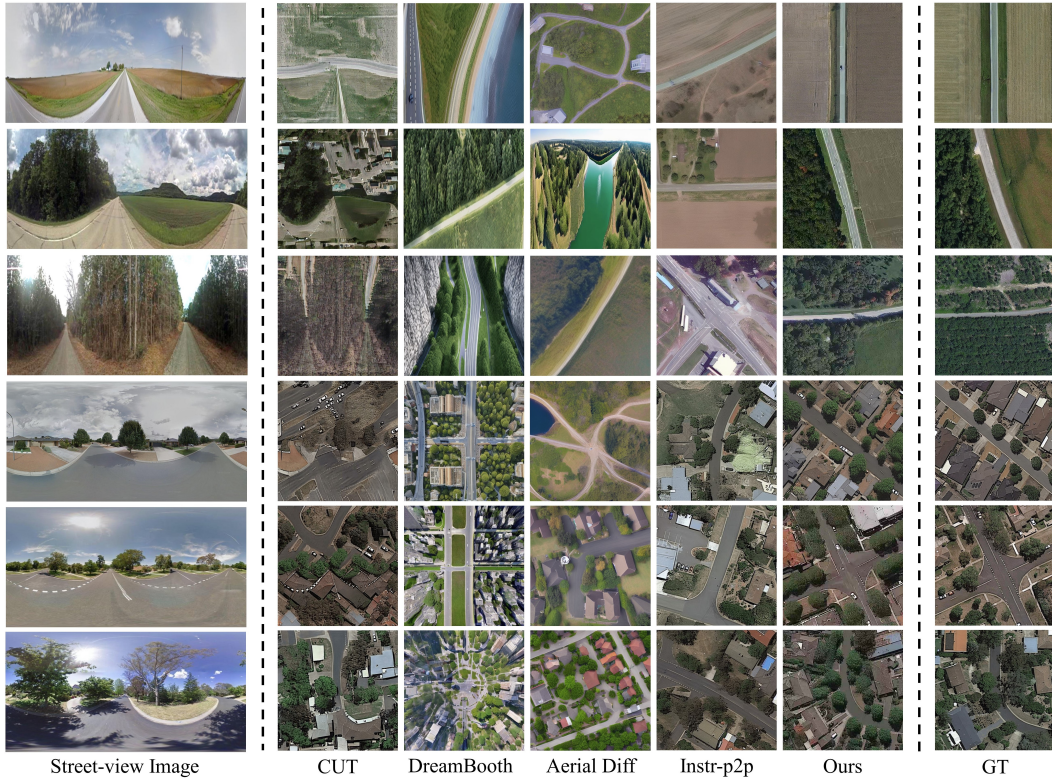


Figure 4: Qualitative comparison of synthesis results for suburban areas. Rows 1-3 show the results on the CVUSA dataset, and rows 4-6 show the results on the CVACT dataset.

In the urban VIGOR-Chicago dataset, SkyDiffusion achieved excellent performance with a 36.6% reduction in FID and a 20.5% improvement in SSIM compared to the state-of-the-art method. The visual results in Fig. 5 show that our method maintains consistent associative information such as crosswalks and lanes. While the non-associative information on building rooftops cannot be consistently generated, it still produces reasonable and realistic results.

4.4 Cross-Dataset Generalization

We trained the model on VIGOR [46] and tested it on the CVACT [18], and vice versa, to evaluate cross-dataset generation capability. Figure 6 shows the cross-dataset generation results of SkyDiffusion. The aim of this task is not to generate identical satellite images but to create scenes with consistent content layouts while exhibiting distinctly different styles. The visualization of the experimental results demonstrates that our method effectively preserves scene content such as road directions and intersections. Additionally, the images processed with the light manipulation module maintain the original content while better matching the illumination conditions of the target domain.



Figure 5: Qualitative comparison of synthesis results for urban areas (VIGOR-Chicago).

Table 2: Quantitative comparison of different methods on VIGOR-Chicago.

Method	Chicago			
	FID (\downarrow)	SSIM (\uparrow)	PSNR (\uparrow)	LPIPS (\downarrow)
CUT [21]	69.63	0.171	13.82	0.666
Aerial Diff [14]	123.16	0.141	11.49	0.831
DreamBooth[27]	132.16	0.116	9.70	0.754
Hawkl [15]	123.47	0.124	9.67	0.752
img2img-turbo [22]	80.10	0.135	11.28	0.690
Instr-p2p [1]	50.30	0.163	10.62	0.689
Ours(One-to-One)	46.35	0.185	10.48	0.665
Ours(Multi-to-One)	31.90	0.205	11.15	0.651

Table 3: Quantitative comparison of cross-dataset generalization test.

Method	Cross-dataset			
	FID (\downarrow)	SSIM (\uparrow)	PSNR (\uparrow)	LPIPS (\downarrow)
CVACT \rightarrow VIGOR-Chicago				
CUT [21]	146.72	0.130	8.55	0.727
Ours (w/o light)	89.76	0.155	9.45	0.739
Ours	63.04	0.162	11.24	0.723
VIGOR-Chicago \rightarrow CVACT				
CUT [21]	132.87	0.107	8.22	0.737
Ours (w/o light)	107.58	0.116	8.76	0.751
Ours	100.58	0.121	11.36	0.714

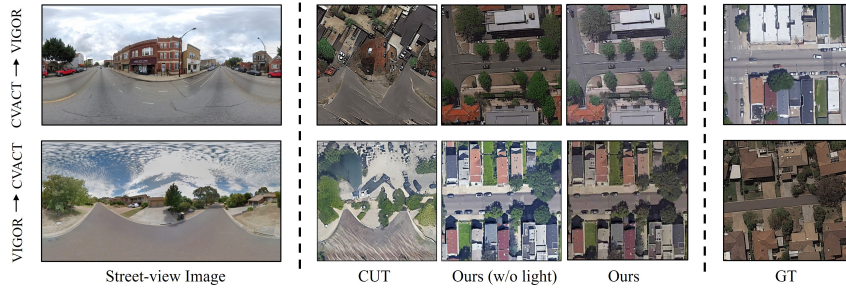


Figure 6: Qualitative comparison of synthesis results for cross-dataset generalization.

Notably, we achieve this by using only a single random image from the training set of the target dataset to obtain the lighting conditions. However, due to the completely different architectural styles of the cities in the CVACT and VIGOR datasets, and because the models are trained on a single dataset, the generalization ability requires further improvement.

4.5 Ablation Study

Curved-BEV controlled synthesis. We conducted ablation experiments on the CVACT dataset, with results shown in Table 4. By comparing the performance of different methods using Curved-BEV and street view inputs, we demonstrate that Curved-BEV consistently enhances performance across various architectures. Additionally, the proposed diffusion method achieves the best results. Further comparisons between existing BEV and Curved-BEV can be found in the supplementary materials.

Furthermore, the **Multi-to-one** method significantly improves metrics compared to the one-to-one mapping, demonstrating its effectiveness in dense urban scenes (Table 2). As shown in the visual results in Figure 7, using multiple street-view images for multi-to-one BEV mapping effectively

Table 4: Ablation study of different modules on CVACT. "Street" represents directly using street-view image inputs, "Curved-BEV" denotes using Curved-BEV transformation, and "Light" stands for the Light Manipulation module.

Method	Options			CVACT			
	Street	Curved-BEV	Light	FID (↓)	SSIM (↑)	PSNR (↑)	LPIPS (↓)
CUT [21]	✓			62.34	0.101	13.02	0.662
CUT [21]		✓		51.71	0.121	13.14	0.658
Aerial Diff [14]	✓			127.29	0.108	10.24	0.878
Aerial Diff [14]		✓		83.34	0.114	11.15	0.831
Ours	✓			62.21	0.115	11.95	0.682
Ours	✓		✓	63.60	0.118	13.49	0.681
Ours		✓		36.48	0.117	13.19	0.642
Ours		✓	✓	35.51	0.123	13.58	0.657

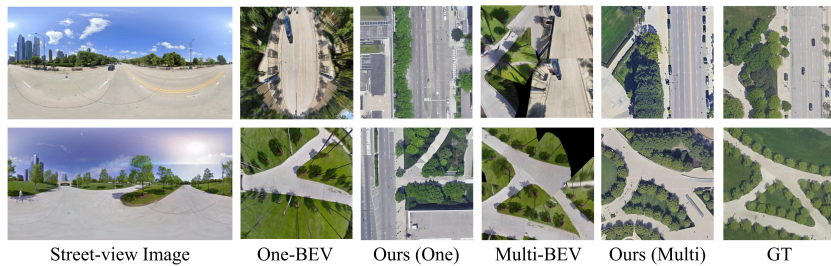


Figure 7: Qualitative comparison of synthesis results for One-to-one and Multi-to-one BEV.

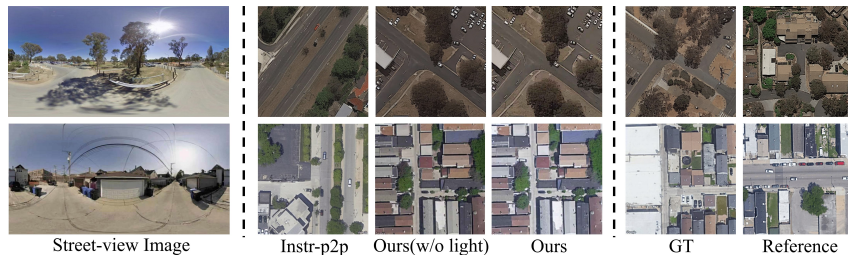


Figure 8: Qualitative analysis of ablation results for light manipulation.

addresses occlusions from tall objects like trees and buildings. This method effectively enhances the BEV sensing range in urban environments, facilitating the generation of large-scale satellite scenes.

Light manipulation. The ablation experiments in Table 4 and the cross-dataset generation results in Table 3 indicate that the Light Manipulation module aligns the lighting conditions of the synthesized images with those of the target domain images, significantly improving SSIM and PSNR metrics. The visualization results in Figure 8 further support this. This improvement is due to the consistent lighting conditions in the satellite data from CVACT and VIGOR-Chicago, which were captured in the same city. Using a small satellite image slice as a reference effectively captures the lighting conditions at the time of capture. Details on this module can be found in the supplementary materials.

5 Conclusion

In this study, we introduce SkyDiffusion, a novel approach specifically designed for street images to satellite images cross-view synthesis. The network operates solely with street images as input, utilizing a curved BEV method and diffusion models to generate realistic and content-consistent satellite images, similar to looking down from the sky. SkyDiffusion achieves state-of-the-art performance in both content consistency and image realism on suburban (CVUSA & CVACT) and urban (VIGOR-Chicago) cross-view datasets, demonstrating significant potential in real-world image synthesis in complex application scenes.

References

- [1] T. Brooks, A. Holynski, and A. A. Efros. Instructpix2pix: Learning to follow image editing instructions. In *Proceedings of the IEEE/CVF Conference on Computer Vision and Pattern Recognition*, pages 18392–18402, 2023.
- [2] X. Chen, H. Ma, J. Wan, B. Li, and T. Xia. Multi-view 3d object detection network for autonomous driving. In *Proceedings of the IEEE conference on Computer Vision and Pattern Recognition*, pages 1907–1915, 2017.
- [3] R. Emmaneel, M. R. Oswald, S. de Haan, and D. Datcu. Cross-view outdoor localization in augmented reality by fusing map and satellite data. *Applied Sciences*, 13(20):11215, 2023.
- [4] F. Fervers, S. Bullinger, C. Bodensteiner, M. Arens, and R. Stiefelhagen. C-bev: Contrastive bird’s eye view training for cross-view image retrieval and 3-dof pose estimation. *arXiv preprint arXiv:2312.08060*, 2023.
- [5] R. Gao, K. Chen, E. Xie, H. Lanqing, Z. Li, D.-Y. Yeung, and Q. Xu. Magicdrive: Street view generation with diverse 3d geometry control. In *International Conference on Learning Representations*, 2024.
- [6] J. Gu, A. Trevisan, K.-E. Lin, J. M. Susskind, C. Theobalt, L. Liu, and R. Ramamoorthi. Nerfdiff: Single-image view synthesis with nerf-guided distillation from 3d-aware diffusion. In *International Conference on Machine Learning*, pages 11808–11826. PMLR, 2023.
- [7] X.-F. Han, H. Laga, and M. Bannour. Image-based 3d object reconstruction: State-of-the-art and trends in the deep learning era. *IEEE transactions on pattern analysis and machine intelligence*, 43(5):1578–1604, 2019.
- [8] M. Heusel, H. Ramsauer, T. Unterthiner, B. Nessler, and S. Hochreiter. Gans trained by a two time-scale update rule converge to a local nash equilibrium. In I. Guyon, U. V. Luxburg, S. Bengio, H. Wallach, R. Fergus, S. Vishwanathan, and R. Garnett, editors, *Advances in Neural Information Processing Systems*, volume 30. Curran Associates, Inc., 2017.
- [9] J. Ho, A. Jain, and P. Abbeel. Denoising diffusion probabilistic models. In H. Larochelle, M. Ranzato, R. Hadsell, M. Balcan, and H. Lin, editors, *Advances in Neural Information Processing Systems*, volume 33, pages 6840–6851. Curran Associates, Inc., 2020.
- [10] J. Ho and T. Salimans. Classifier-free diffusion guidance. *arXiv preprint arXiv:2207.12598*, 2022.
- [11] B. Kawar, S. Zada, O. Lang, O. Tov, H. Chang, T. Dekel, I. Mosseri, and M. Irani. Imagic: Text-based real image editing with diffusion models. In *Proceedings of the IEEE/CVF Conference on Computer Vision and Pattern Recognition*, pages 6007–6017, 2023.
- [12] Z. Ke, Y. Liu, L. Zhu, N. Zhao, and R. W. Lau. Neural preset for color style transfer. In *Proceedings of the IEEE/CVF Conference on Computer Vision and Pattern Recognition*, pages 14173–14182, 2023.
- [13] Z. Ke, C. Sun, L. Zhu, K. Xu, and R. W. Lau. Harmonizer: Learning to perform white-box image and video harmonization. In *European Conference on Computer Vision*, pages 690–706. Springer, 2022.
- [14] D. Kothandaraman, T. Zhou, M. Lin, and D. Manocha. Aerial diffusion: Text guided ground-to-aerial view synthesis from a single image using diffusion models. In *SIGGRAPH Asia 2023 Technical Communications*, pages 1–4. 2023.
- [15] D. Kothandaraman, T. Zhou, M. C. Lin, and D. Manocha. Hawki: Homography&mutual information guidance for 3d-free single image to aerial view. 2023.
- [16] B. Li, K. Xue, B. Liu, and Y.-K. Lai. Bbim: Image-to-image translation with brownian bridge diffusion models. In *Proceedings of the IEEE/CVF conference on computer vision and pattern recognition*, pages 1952–1961, 2023.

- [17] Z. Li, W. Wang, H. Li, E. Xie, C. Sima, T. Lu, Y. Qiao, and J. Dai. Bevformer: Learning bird’s-eye-view representation from multi-camera images via spatiotemporal transformers. In *European conference on computer vision*, pages 1–18. Springer, 2022.
- [18] L. Liu and H. Li. Lending orientation to neural networks for cross-view geo-localization. In *Proceedings of the IEEE/CVF conference on computer vision and pattern recognition*, pages 5624–5633, 2019.
- [19] R. Liu, R. Wu, B. Van Hoorick, P. Tokmakov, S. Zakharov, and C. Vondrick. Zero-1-to-3: Zero-shot one image to 3d object. In *Proceedings of the IEEE/CVF International Conference on Computer Vision*, pages 9298–9309, 2023.
- [20] X. Lu, Z. Li, Z. Cui, M. R. Oswald, M. Pollefeys, and R. Qin. Geometry-aware satellite-to-ground image synthesis for urban areas. In *Proceedings of the IEEE/CVF Conference on Computer Vision and Pattern Recognition*, pages 859–867, 2020.
- [21] T. Park, A. A. Efros, R. Zhang, and J.-Y. Zhu. Contrastive learning for unpaired image-to-image translation. In *Computer Vision—ECCV 2020: 16th European Conference, Glasgow, UK, August 23–28, 2020, Proceedings, Part IX 16*, pages 319–345. Springer, 2020.
- [22] G. Parmar, T. Park, S. Narasimhan, and J.-Y. Zhu. One-step image translation with text-to-image models. *arXiv preprint arXiv:2403.12036*, 2024.
- [23] M. Qian, J. Xiong, G.-S. Xia, and N. Xue. Sat2density: Faithful density learning from satellite-ground image pairs. In *Proceedings of the IEEE/CVF International Conference on Computer Vision (ICCV)*, pages 3683–3692, October 2023.
- [24] K. Regmi and A. Borji. Cross-view image synthesis using conditional gans. In *Proceedings of the IEEE conference on Computer Vision and Pattern Recognition*, pages 3501–3510, 2018.
- [25] K. Regmi and A. Borji. Cross-view image synthesis using geometry-guided conditional gans. *Computer Vision and Image Understanding*, 187:102788, 2019.
- [26] R. Rombach, A. Blattmann, D. Lorenz, P. Esser, and B. Ommer. High-resolution image synthesis with latent diffusion models. In *Proceedings of the IEEE/CVF conference on computer vision and pattern recognition*, pages 10684–10695, 2022.
- [27] N. Ruiz, Y. Li, V. Jampani, Y. Pritch, M. Rubinstein, and K. Aberman. Dreambooth: Fine tuning text-to-image diffusion models for subject-driven generation. In *Proceedings of the IEEE/CVF Conference on Computer Vision and Pattern Recognition*, pages 22500–22510, 2023.
- [28] P.-E. Sarlin, D. DeTone, T.-Y. Yang, A. Avetisyan, J. Straub, T. Malisiewicz, S. R. Bulò, R. Newcombe, P. Kotschieder, and V. Balntas. Orienternet: Visual localization in 2d public maps with neural matching. In *Proceedings of the IEEE/CVF Conference on Computer Vision and Pattern Recognition*, pages 21632–21642, 2023.
- [29] R. Shi, H. Chen, Z. Zhang, M. Liu, C. Xu, X. Wei, L. Chen, C. Zeng, and H. Su. Zero123++: a single image to consistent multi-view diffusion base model. *arXiv preprint arXiv:2310.15110*, 2023.
- [30] Y. Shi, D. Campbell, X. Yu, and H. Li. Geometry-guided street-view panorama synthesis from satellite imagery. *IEEE Transactions on Pattern Analysis and Machine Intelligence*, 44(12):10009–10022, 2022.
- [31] Y. Shi, L. Liu, X. Yu, and H. Li. Spatial-aware feature aggregation for image based cross-view geo-localization. *Advances in Neural Information Processing Systems*, 32, 2019.
- [32] Y. Shi, F. Wu, A. Perincherry, A. Vora, and H. Li. Boosting 3-dof ground-to-satellite camera localization accuracy via geometry-guided cross-view transformer. In *Proceedings of the IEEE/CVF International Conference on Computer Vision*, pages 21516–21526, 2023.
- [33] J. Song, C. Meng, and S. Ermon. Denoising diffusion implicit models. In *International Conference on Learning Representations*, 2021.

- [34] Z. Song, J. Lu, Y. Shi, et al. Learning dense flow field for highly-accurate cross-view camera localization. *Advances in Neural Information Processing Systems*, 36, 2023.
- [35] H. Tang, D. Xu, N. Sebe, Y. Wang, J. J. Corso, and Y. Yan. Multi-channel attention selection gan with cascaded semantic guidance for cross-view image translation. In *Proceedings of the IEEE/CVF conference on computer vision and pattern recognition*, pages 2417–2426, 2019.
- [36] S. Tang, F. Zhang, J. Chen, P. Wang, and Y. Furukawa. MVDiffusion: Enabling holistic multi-view image generation with correspondence-aware diffusion. In *Thirty-seventh Conference on Neural Information Processing Systems*, 2023.
- [37] Z. Teng, J. Zhang, K. Yang, K. Peng, H. Shi, S. Reiß, K. Cao, and R. Stiefelhagen. 360bev: Panoramic semantic mapping for indoor bird’s-eye view. In *Proceedings of the IEEE/CVF Winter Conference on Applications of Computer Vision*, pages 373–382, 2024.
- [38] A. Toker, Q. Zhou, M. Maximov, and L. Leal-Taixé. Coming down to earth: Satellite-to-street view synthesis for geo-localization. In *Proceedings of the IEEE/CVF Conference on Computer Vision and Pattern Recognition*, pages 6488–6497, 2021.
- [39] H.-Y. Tseng, Q. Li, C. Kim, S. Alsisan, J.-B. Huang, and J. Kopf. Consistent view synthesis with pose-guided diffusion models. In *Proceedings of the IEEE/CVF Conference on Computer Vision and Pattern Recognition*, pages 16773–16783, 2023.
- [40] D. Wang, X. Cui, X. Chen, Z. Zou, T. Shi, S. Salcudean, Z. J. Wang, and R. Ward. Multi-view 3d reconstruction with transformers. In *Proceedings of the IEEE/CVF international conference on computer vision*, pages 5722–5731, 2021.
- [41] X. Wang, R. Xu, Z. Cui, Z. Wan, and Y. Zhang. Fine-grained cross-view geo-localization using a correlation-aware homography estimator. *Advances in Neural Information Processing Systems*, 36, 2023.
- [42] S. Workman, R. Souvenir, and N. Jacobs. Wide-area image geolocation with aerial reference imagery. In *Proceedings of the IEEE International Conference on Computer Vision*, pages 3961–3969, 2015.
- [43] S. Wu, H. Tang, X.-Y. Jing, H. Zhao, J. Qian, N. Sebe, and Y. Yan. Cross-view panorama image synthesis. *IEEE Transactions on Multimedia*, 2022.
- [44] J. Ye, Q. Luo, J. Yu, H. Zhong, Z. Zheng, C. He, and W. Li. Sg-bev: Satellite-guided bev fusion for cross-view semantic segmentation. *arXiv preprint arXiv:2404.02638*, 2024.
- [45] L. Zhang, A. Rao, and M. Agrawala. Adding conditional control to text-to-image diffusion models. In *Proceedings of the IEEE/CVF International Conference on Computer Vision (ICCV)*, pages 3836–3847, October 2023.
- [46] S. Zhu, T. Yang, and C. Chen. Vigor: Cross-view image geo-localization beyond one-to-one retrieval. In *Proceedings of the IEEE/CVF Conference on Computer Vision and Pattern Recognition*, pages 3640–3649, 2021.
- [47] Y. Zhu, S. Chen, X. Lu, and J. Chen. Cross-view image synthesis from a single image with progressive parallel gan. *IEEE Transactions on Geoscience and Remote Sensing*, 2023.